# Blind Deblurring Using Internal Patch Recurrence: Supplamentary Material

Tomer Michaeli and Michal Irani

Dept. of Computer Science and Applied Mathematics
Weizmann Institute of Science, Israel

**1.** We discuss the mapping between the error-ratio measure computed with the nonblind deblurring algorithm of Levin *et al.* [11] and the error-ratio measure computed with the nonblind-deblurring method of Zoran and Weiss [22].

**2.** We explain why down-sampling an image using a $\mathrm{sinc}$ kernel has an effect of aliasing-aware sharpening.

## 1 Mapping Between Different Types of Error Ratios

The error-ratio measure $r$ (Eq. (15) in the paper), which is standardly used to quantify the performance of blind-deblurring methods, depends on the type of non-blind deblurring algorithm used for the final deblurring stage. The error-ratios reported in our paper (and also used in [18]) were computed with the current state-of-the-art non-blind deblurring method of Zoran and Weiss [22]. Previous studies (*e.g.,* [12,13]) reported error-ratios computed with the non-blind deblurring method of Levin *et al.* [11] (the state-of-the-art at that time). In the figure below we re-plot the cumulative distribution of error-ratios, but this time computed with [11]. As can be seen, the *absolute* error-ratio values are different than those in the corresponding graph (Fig. 5 in the paper) of error-ratios computed with [22]. Nonetheless, the two graphs reflect the same *relative* behavior of all the methods.

In the table below we report the average performance, worst-case performance and success rate of all algorithms, this time using error-ratios computed with the non-blind deblurring of [11]. We note that for this setting, the *blind deblurring* paper of Levin *et al.* [13] reported a threshold of $3$ between good and bad visual results. Consequently, we regard success rate in this context as the percent of images with error-ratio smaller than $3$. As in the corresponding table (Table 1 in the paper) of error-ratios computed with the non-blind deblurring of [22], this table shows that our method and the method of Sun *et al.* [18] outperform all other methods in all three categories. The average performance of our method is close to that of Sun *et al.* [18], while our worst-case performance is significantly better. Note that also when using this measure, only three methods (the same three) attain an *average* error ratio smaller than $3$: Our method, Sun *et al.* [18], Xu and Jia [19].

The figure below further shows a scatter-plot of both types of error-ratios. Each point in this plot corresponds to a kernel produced by one of the $7$ tested blind-deblurring methods on one of the $640$ blurry images in the database (once used with the non-blind deblurring of [22] and once with the non-blind deblurring of [11]). In other words, $4480$

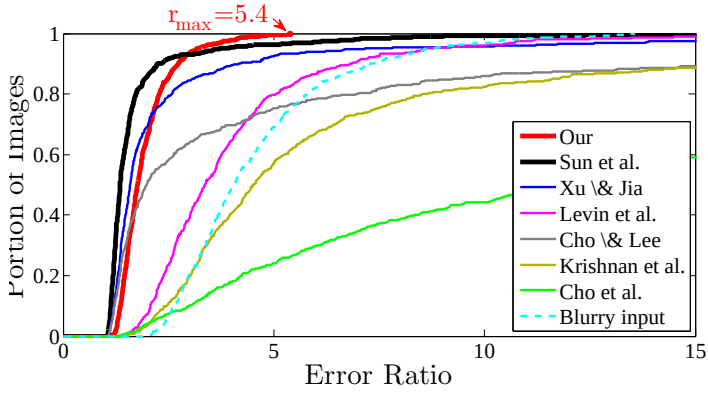


**Figure:** ***Cumulative distribution of error ratios (similar to Fig. 5 in the paper), but this time the error-ratios are computed with the nonblind deblurring algorithm of Levin*** *et al.* ***[11].***

**Table:** ***Quantitative comparison of all methods over the entire database*** (640 ***blurry images), based on error-ratios computed with [11]***

| | **Average performance** (mean error ratio) | **Worst-case performance** (highest error-ratio) | **Success rate** (percent of images with error ratio $< 3$) |
|---|---|---|---|
| **Our** | 1.9 | **5.4** | **93.3%** |
| Sun *et al.* [18] | **1.8** | 17.2 | 93.1% |
| Xu & Jia [19] | 2.7 | 60.4 | 84.5% |
| Levin *et al.* [13] | 4.1 | 26.5 | 46.7% |
| Cho & Lee [1] | 6.5 | 107.9 | 64.1% |
| Krishnan *et al.* [10] | 8.8 | 167.5 | 20.5% |
| Cho *et al.* [2] | 19.7 | 145.9 | 23.8% |

points ($640 \times 7$). This figure indicates that there is very strong correlation between the error-ratios computed with [22] and those computed with [11]. The best linear fit (shown in red) suggests that an error ratio of 3 with [11] corresponds to an error-ratio of approximately 5 with [22]. This further supports our visual observations that an error-ratio of approximately 5 with [22] corresponds to the threshold between good and bad visual results.

## 2 Aliasing-Aware Sharpening by a Factor of $\alpha$

For simplicity, we focus on 1D signals. The extension to 2D is trivial. Suppose that the continuous-space scene is convolved with a continuous-space kernel $k(\xi)$ and sampled at integer locations to yield the discrete-space blurry image[1] $y[n]$. Let $f(\xi)$ be a small pattern in the scene that recurs elsewhere $\alpha$-times larger as $f(\xi/\alpha)$ for some factor

[1] We use parentheses for continuous-space signals and square brackets for discrete-space signals.

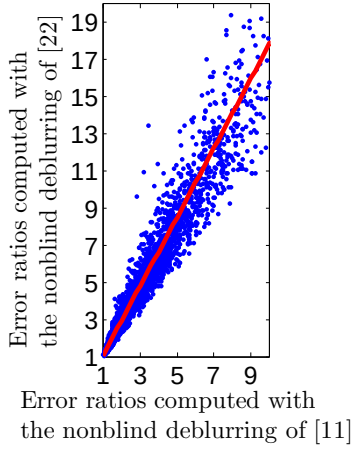


**Figure:** ***Error ratios computed with the nonblind deblurring algorithm Zoran and Weiss [22] vs. error ratios computed with the nonblind deblurring algorithm of Levin*** *et al.* ***[11].***

$\alpha > 1$. These two regions appear in the image as two patches:

$$q[n] = \int f(\xi)k(n-\xi)d\xi, \tag{1}$$

$$r[n] = \int f(\xi/\alpha)k(n-\xi)d\xi. \tag{2}$$

We assume that $k(\xi)$ is bandlimited to $\pi$, so that no aliasing occurs when sampling the continuous scene (*i.e.,* we assume the blurry input image is aliasing free). This implies that the discrete-space Fourier transforms (DSFTs) of $q[n]$ and $r[n]$ are given by[2]

$$Q\left(e^{i\omega}\right) = F(\omega)K(\omega), \quad -\pi \le \omega \le \pi \tag{3}$$

$$R\left(e^{i\omega}\right) = \alpha F(\alpha\omega)K(\omega), \quad -\pi \le \omega \le \pi \tag{4}$$

where $F(\omega)$ and $K(\omega)$ are the continuous-space Fourier transforms (CSFTs) of the pattern $f(\xi)$ and the kernel $k(\xi)$, respectively.

Consider the following $\alpha$-times coarser version of $r[n]$, which we obtain by re-sampling $r[n]$ on the grid $\{\alpha n\}_{n\in\mathbb{Z}}$ with an ideal sinc kernel:

$$r^{\alpha}[n] = \sum_{m} r[m]\frac{1}{\alpha}\,\mathrm{sinc}\left(\frac{m\alpha - n}{\alpha}\right). \tag{5}$$

As we show below (see the subsection on "Sinc Re-Sampling"), the DSFT of $r^{\alpha}[n]$ is given by

$$R^{\alpha}\left(e^{i\omega}\right) = \frac{1}{\alpha}R\left(e^{i\omega/\alpha}\right), \quad -\pi \le \omega \le \pi. \tag{6}$$

[2] We use the argument $e^{i\omega}$ in DSFTs as a reminder that they are $2\pi$-periodic. Furthermore, we always specify the contents of DSFTs only for $\omega \in [-\pi, \pi]$. Values outside this range are obtained by a $2\pi$-periodic extension.

Substituting (4) into (6), we have that

$$R^{\alpha}\left(e^{i\omega}\right) = F(\omega)K(\omega/\alpha), \quad -\pi \leq \omega \leq \pi. \tag{7}$$

Thus, $r^{\alpha}[n]$ corresponds to samples of the continuous pattern $f(\xi)$, after it has been convolved with $K(\omega/\alpha)\,\mathrm{rect}(\omega)$, where $\mathrm{rect}(\omega) = 1$ for $\omega < \pi$, and is zero elsewhere (the CSFT of $\mathrm{sinc}(\xi)$). In other words, $r^{\alpha}[n]$ is exactly the *aliasing-aware $\alpha$-times sharper version of* $q[n]$. This is visualized in the figure below.

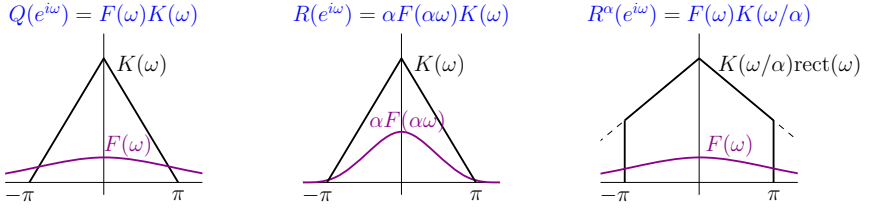


**Figure:** ***Formation of the discrete-space Fourier transforms of the patches*** $q[n]$, $r[n]$, ***and*** $r^{\alpha}[n]$, ***from the continuous-space Fourier transforms of*** $f(\xi)$ ***and*** $k(\xi)$. The patches $r^{\alpha}[n]$ and $q[n]$ correspond to samples of the same continuous-space structure $f(\xi)$, but filtered with different kernels. The patch $q[n]$ is associated with the blur $K(\omega)$, while the patch $r^{\alpha}[n]$ is associated with the aliasing-aware blur $K(\omega/\alpha)\,\mathrm{rect}(\omega)$.

### 2.1 Sinc Re-Sampling

To prove (6), note that we can write the sinc resampling formula (5) as

$$r^{\alpha}[n] = \tilde{r}(n\alpha), \tag{8}$$

where $\tilde{r}(\xi)$ is the continuous-space interpolated signal

$$\tilde{r}(\xi) = \sum_{n} r[n]\frac{1}{\alpha}\,\mathrm{sinc}\left(\frac{\xi - n}{\alpha}\right). \tag{9}$$

Now, the CSFT of $\tilde{r}(\xi)$ is given by

$$\begin{aligned}
\tilde{R}(\omega) &= \int \left(\sum_{n} r[n]\frac{1}{\alpha}\,\mathrm{sinc}\left(\frac{\xi - n}{\alpha}\right)\right) e^{-i\omega\xi} d\xi \\
&= \sum_{n} r[n]\frac{1}{\alpha}\int \mathrm{sinc}\left(\frac{\xi - n}{\alpha}\right) e^{-i\omega\xi} d\xi \\
&= \sum_{n} r[n]\,\mathrm{rect}(\alpha\omega)e^{-i\omega n} \\
&= \mathrm{rect}(\alpha\omega)\sum_{n} r[n]e^{-i\omega n} \\
&= \mathrm{rect}(\alpha\omega)R\left(e^{i\omega}\right),
\end{aligned} \tag{10}$$

where $R\left(e^{i\omega}\right)$ is the DSFT of $r[n]$. Since $\tilde{R}(\omega)$ is bandlimited to $\pi/\alpha$, sampling it on the grid $\{\alpha n\}_{n\in\mathbb{Z}}$ introduces no aliasing. Therefore, according to the Shannon Sampling Theorem, the DSFT of $r^{\alpha}[n]$ is given by

$$R^{\alpha}(e^{i\omega}) = \frac{1}{\alpha}\tilde{R}\left(\frac{\omega}{\alpha}\right) = \frac{1}{\alpha}R\left(e^{i\omega/\alpha}\right), \quad -\pi \leq \omega \leq \pi, \tag{11}$$

proving (6).